ACS Partner Journal
PRECISION CHEMISTRY
pubs.acs.org/PrecisionChem

Article

Side-Chain Type Ferrocene Macrocycles

Bin Lan, Jindong Xu, Lingyun Zhu, Xinyu Chen, Hideya Kono, Peihan Wang, Xin Zuo, Jianfeng Yan, Akiko Yagi, Yongshen Zheng, Songhua Chen,* Yaofeng Yuan,* Kenichiro Itami,* and Yuanming Li*

Cite This: *Precis. Chem.* 2024, 2, 143−150

Read Online

ACCESS | Metrics & More | Article Recommendations | Supporting Information

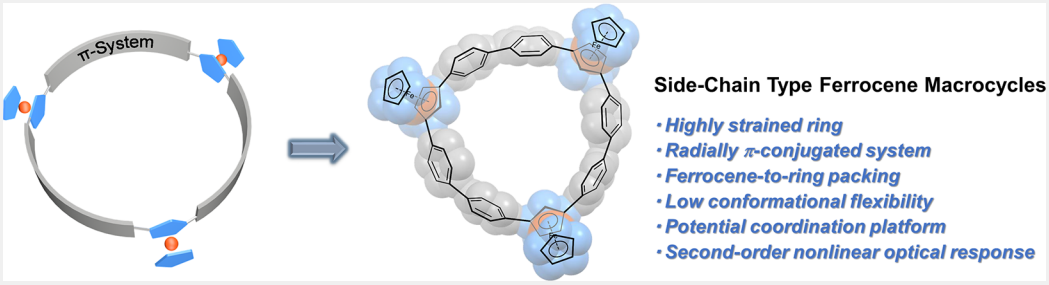

ABSTRACT: A class of side-chain type ferrocene macrocycles with a radially conjugated system is introduced in this study. The stereo configurations of these ferrocene rings were determined through single-crystal X-ray diffraction analysis. Notably, in the solid state, the ferrocene rings exhibit a distinctive herringbone stacking pattern imposed by a ferrocene-to-ring host−guest interaction. Through UV−vis absorption spectroscopy, electrochemical measurements, and theoretical calculations, valuable insights into the electronic properties of these rings were obtained. In addition, the single crystal of macrocycle $\mathbf{A_2B}$ demonstrates a second-order nonlinear optical response. As a class of organometallic nanorings, this work holds great potential for further exploration in the fields of organometallic chemistry, molecular electronics, and host−guest chemistry.

KEYWORDS: *Ferrocene, Conjugated Macrocycles, Organometallic Macrocycles, Second-Order Nonlinear Optical, Nanoring*

INTRODUCTION

Ferrocene-based polymers are attractive materials for potential use in optoelectronic devices (Figure 1a).[1−6] Symmetrical conjugated cyclic structures not only are aesthetically captivating, but also add unique properties, such as enhanced π-conjugation, solubility, and host−guest interaction, when compared to their noncyclic counterparts.[7−17] Among these structures, ferrocene-based macrocycles have garnered significant attention in the fields of molecular machinery,[18,19] molecular electronics,[20−22] and redox-active supramolecular systems.[23−26] Drawing inspiration from the paradigm of ferrocene-based polymers,[26−28] ferrocene-based π-conjugated macrocycles can be categorized into two types: main-chain macrocycles and side-chain macrocycles (Figure 1b). In main-chain macrocycles, the transition metal is an integral component of the macrocycle, whereas in side-chain macrocycles, the transition metal is coordinated to the backbone of the macrocycle.

To date, the main-chain macrocycles incorporating ferrocene units usually feature 1,1′-disubstituted ferrocene units[29,30] and conjugated linkages, such as pyrene[31,32] or 1,3-diethynylbenzene[33−35] (Figure 1c). The inherent rotation of the cyclopentadienyl (Cp) ring in ferrocene likely contributes to the formation of these twisted systems by reducing the strain. These strainless rings exhibit mixed-valence properties, as well as high solubility. We noted that the side-chain macrocyclic species with 1,2-[36] or 1,3-disubstituted[37,38] ferrocene modules are much rarer. Macrocycles of this type typically exhibit varied stereoisomerism due to the different orientations of the CpFe group. To fundamentally understand the relationship between organometallic fragment orientation and electronic structure, side-chained ferrocene macrocycles are considered as suitable candidates. In addition, the dissociation of CpFe fragments from the incorporated ferrocenes in side-chain type macrocycles can lead to Cp-embedded macrocycles,[39−41] which would be a new coordination platform for different metals as a curved π-conjugated macrocyclic ligands.[42,43] This encouraged us to pursue the synthesis of side-chain type ferrocene rings.

The electrochemical,[25] aromatic,[30] and supramolecular properties exhibited by these macrocycles are closely associated with their shape, as well as the number, proximity, and connectivity of their redox centers.[26] Accordingly, to enrich the functional landscape of side-chain type ferrocene-

Received: December 19, 2023
Revised: February 28, 2024
Accepted: February 28, 2024
Published: March 13, 2024

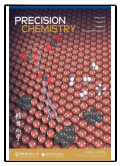

https://doi.org/10.1021/prechem.3c00121
Precis. Chem. 2024, 2, 143−150

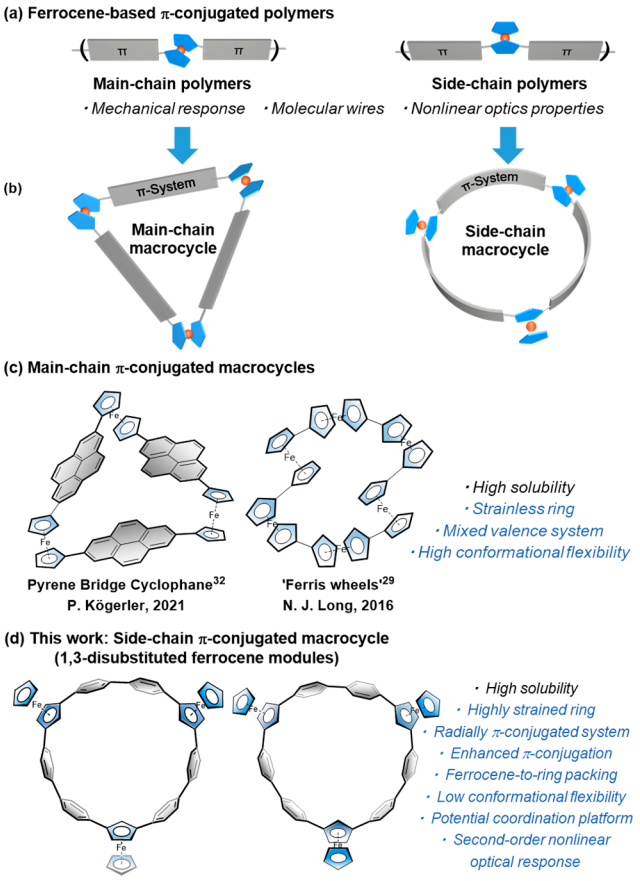

Figure 1. Conceptual representation of (a) ferrocene-based π-conjugated polymers; (b) main-chain and side-chain type ferrocene π-conjugated macrocycles; (c) representative examples of main-chain ferrocene π-conjugated macrocycles; (d) this work: side-chain type radially π-conjugated macrocycles.

based conjugated macrocycles, we now introduce two nanosized conjugated macrocycles with different stereoisomerism by incorporating three or four 1,3-ferrocenylene units and paraphenylenes as linkage to give a new class of organometallic rings,[44−52] which feature radial conjugation, restricted conformation, and enhanced π-conjugation. The unique ferrocene-to-ring host−guest interaction of these macrocycles was determined through single-crystal X-ray diffraction analysis.

RESULTS AND DISCUSSION

Synthesis

The synthesis of the target macrocycles was achieved by the Pt-mediated coupling strategy developed by Bäuerle,[53,54] Yamago,[55] and Isobe et al. (Scheme 1).[56,57] Initially, 1,3-diiodoferrocene **1** was prepared according to the method established by Weissensteiner and co-workers.[58] Subsequently, the macrocyclic precursor diboronic ester **3** was obtained through the Suzuki−Miyaura coupling reaction, followed by Miyaura borylation in 45% total yield. In addition, crystals of compound **2** were obtained by slow evaporation from a solution of the complex in a CH_2Cl_2/*n*-hexane mixture (see Figure S1 for detailed structure information). The transmetalation of compound **3** with $Pt(cod)Cl_2$ in 1,2-dichloroethane (DCE) heated at reflux in the presence of cesium fluoride for 48 h afforded the macrocyclic platinum

Scheme 1. Synthetic Route to Side-Chain Type Ferrocene Rings

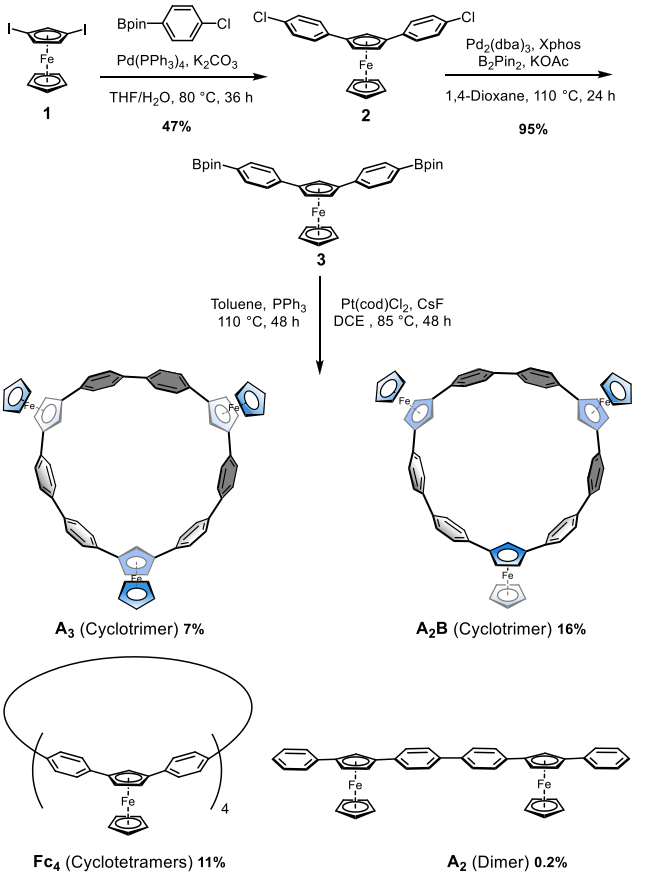

intermediate. Without further purification, the resultant mixture was subjected to reductive elimination conditions to give the target macrocycles, namely, cyclotrimers ($\mathbf{A_2B}$ and $\mathbf{A_3}$) and cyclotetramers ($\mathbf{Fc_4}$).

As anticipated, the incorporation of 1,3-disubstituted ferrocene into the side-chain type macrocycle introduced geometrical isomerism. For the cyclotrimers, the ratio of two possible stereoisomers, $\mathbf{A_2B}$ and $\mathbf{A_3}$, was determined to be 5:2 by using ^{1}H NMR spectroscopy (Figure S53). Both stereoisomers could be separated through repeated silica gel column chromatography, yielding $\mathbf{A_3}$ in 7% yield and $\mathbf{A_2B}$ in 16% yield. The stereoisomers of the cyclotetramers could not be separated using either silica gel column chromatography or gel permeation chromatography (GPC). However, $\mathbf{Fc_4}$ was confirmed by MALDI FT-ICR MS. Additionally, a linear dimer $\mathbf{A_2}$ was also isolated in 0.2% yield.

The ^{1}H NMR spectra of $\mathbf{A_2B}$, $\mathbf{A_3}$, $\mathbf{A_2}$, and $\mathbf{Fc_4}$ were compared to reveal interesting signal shifts of the hydrogen atoms of Cp rings (Figure 2). $\mathbf{A_3}$ exhibited a set of ferrocenyl signals, consistent with the theoretically high $C_{3\,V}$ symmetry, while $\mathbf{A_2B}$ displayed two sets of signals corresponding to C_S symmetry. Upon comparison with $\mathbf{A_2}$, it was observed that the ferrocenyl units in the macrocyclic products exhibited tilting, resulting in progressive upfield shifts of the hydrogen atom signals (H_a and H_b) on Cp embedded in the ring. Specifically, the signal of H_a showed a significant shift of 1.54 ppm for $\mathbf{A_3}$, 1.58 and 1.60 ppm for $\mathbf{A_2B}$, respectively. This upfield shift phenomenon is more pronounced than in main-chain type ferrocene rings.[29] In contrast, the chemical shift of H_c shifted

https://doi.org/10.1021/prechem.3c00121
Precis. Chem. 2024, 2, 143−150

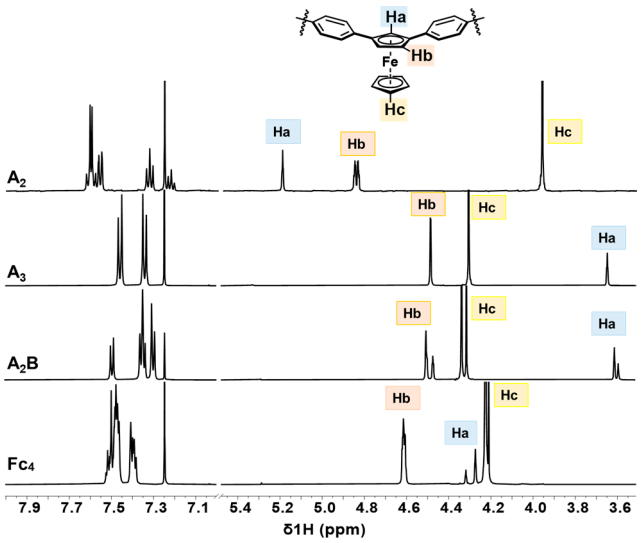

Figure 2. Partial ^{1}H NMR spectra of $\mathbf{A_2}$, $\mathbf{A_3}$, $\mathbf{A_2B}$, and $\mathbf{Fc_4}$ in $CDCl_3$.

downfield as the conformationally flexible Cp rings moved away from the shielding region. Notably, for $\mathbf{Fc_4}$, an increasing ring size led to a gradual convergence of the corresponding signals toward those observed in linear congeners.

X-RAY CRYSTAL STRUCTURES

Single crystals of $\mathbf{A_2B}$ and $\mathbf{A_3}$, suitable for X-ray diffraction analysis, were obtained by slow diffusion of dichloromethane into an *n*-hexane solution, allowing for the unambiguous determination of the stereoconfiguration of the cyclotrimers. As shown in Figure 3b, all three ferrocenyl units are in the same orientation, with respect to the ring plane in $\mathbf{A_3}$. In $\mathbf{A_2B}$, two ferrocenyl units are in a *syn* orientation with each other, while the third ferrocenyl unit is in an *anti*-orientation relative to them. These distinct configurations result in different space groups, $P2_12_12_1$ ($\mathbf{A_2B}$) and $P2_{1/c}$ ($\mathbf{A_3}$). The average diameter of both macrocycles is approximately 12 Å. In $\mathbf{A_2B}$, the rotational angle between the macrocycle plane and the embeded Fc plane is 31.62° for the *anti* ferrocenyl unit, while for the *syn* ferrocenyl units, the angles are 40.17° and 42.59°, respectively. In the case of $\mathbf{A_3}$, these values are close, which are 44.26°, 39.58°, and 42.14°, respectively (see Figures S5 and S10 for detailed measurement reference information). Regarding the tilting of FeCp groups, the angles are 3.49°, 2.56° and 1.68° for $\mathbf{A_3}$, and 3.69° (anti), 1.52° (syn) and 0.62° (syn) for $\mathbf{A_2B}$. Due to tripod-like shape of $\mathbf{A_3}$, reminiscent of ancient Chinese cauldrons, ceremonial vessels known as "ding", $\mathbf{A_3}$ was aptly named "dingarene".

Furthermore, both $\mathbf{A_2B}$ (Figure 3c) and $\mathbf{A_3}$ (Figure S9) displayed a distinctive herringbone stacking pattern imposed by a ferrocene-to-ring host–guest interaction. The ferrocenyl unit in each ring is effectively nestled within the cavity of the neighboring rings, primarily driven by Cp-H-π interactions. In the case of $\mathbf{A_2B}$ ($\mathbf{A_3}$ see Figure S12), the distance between hydrogen atoms and aromatic planes (d_{PLN}), the distance between the carbon atoms and the center of the aromatic planes (d_{C-X}), and the angle at the hydrogen ($\angle$C–H–X) (X represents the centroid of the phenyl) are measured to be 3.1 4.0, and 147.2°, respectively. These values align perfectly with the established C–H–π criteria, demonstrating the presence of these interactions.[59,60] Notably, this observation is consistent

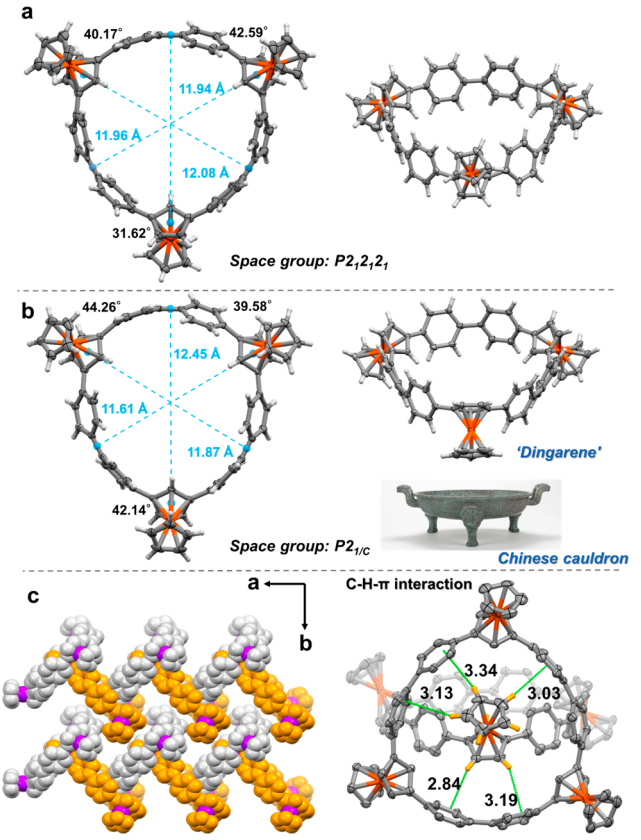

Figure 3. X-ray crystal structures of (a) $\mathbf{A_2B}$ and (b) $\mathbf{A_3}$ (thermal ellipsoids are shown at 50% probability; solvent molecules have been omitted for clarity). (c) Crystal stacking along the *a*-axis of $\mathbf{A_2B}$ and distances between the hydrogen atoms and the aromatic plane (iron atoms, purple).

with the host–guest complexes of FcC[8]cycloparaphenylenes (CPP) that have been recently reported.[61]

REDOX AND PHOTOPHYSICAL PROPERTIES

For multiferrocenyl cyclic systems, electrochemistry serves as a conventional tool for assessing the electronic communication between redox sites.[62,63] In this regard, the redox properties of $\mathbf{A_2B}$ and $\mathbf{A_3}$ were investigated by using cyclic voltammetry (CV) and differential pulse voltammetry (DPV). Initially, the CV of $\mathbf{A_2B}$ and $\mathbf{A_3}$ in 0.1 M [*n*-Bu_4N][PF_6]/CH_2Cl_2 were examined, revealing a single reversible redox wave for both compounds (Figure S13). In an attempt to enhance the splitting of the redox potentials, we substituted the electrolyte with [*n*-Bu_4N][BArF] (BArF = tetrakis[3,5-bis-(trifluoromethyl)phenyl]borate), as BArF exhibits a weak ion-pairing ability and increased electrostatic interaction.[64,65] However, this modification also resulted in only one unresolved wave in the CV (Figure S14). Finally, by further replacing the cations with Na^+, two unresolved waves were observed in 0.01 M [Na][BArF]/CH_2Cl_2 (Figure 4).[66,67] The lack of a clear splitting between the oxidation waves suggests weak electronic communication between ferrocenyl units,[68,69] which is likely due to the large iron–iron geometric distance.[70] The lack of electronic interactions was verified further by the absence of any detectable intervalence charge transfer band in redox titrations (Figures S32 and S33).

The UV–vis absorption spectra of $\mathbf{A_2}$, $\mathbf{A_2B}$ and $\mathbf{A_3}$ recorded in CH_2Cl_2 are shown in Figure 5. $\mathbf{A_2B}$ exhibits a maximum

https://doi.org/10.1021/prechem.3c00121
Precis. Chem. 2024, 2, 143–150

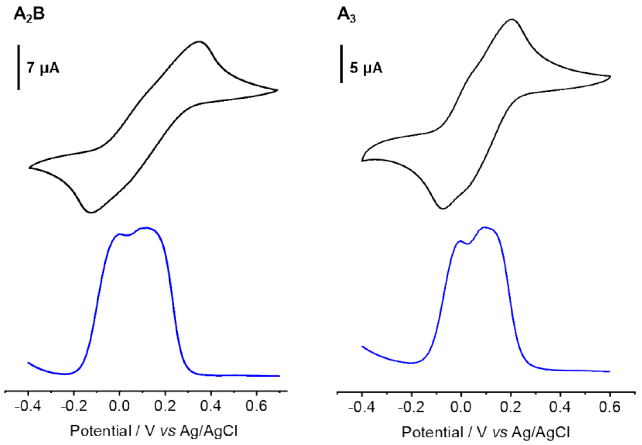

Figure 4. Cyclic voltammetry (CV, top) and differential pulse voltammetry (DPV, bottom) were recorded in 0.01 M [Na][BArF]/CH_2Cl_2.

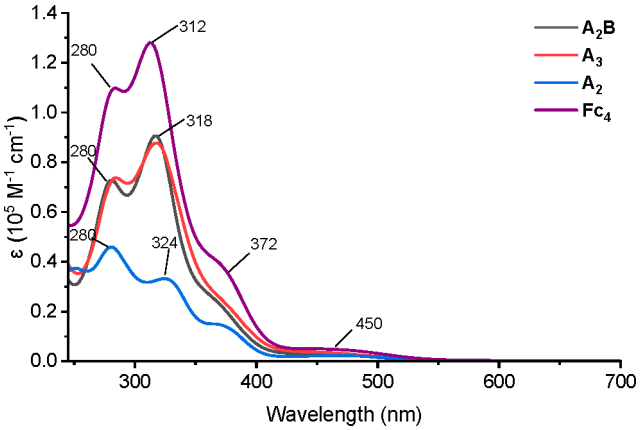

Figure 5. UV−vis absorption spectra of $\mathbf{A_2B}$, $\mathbf{A_3}$, $\mathbf{A_2}$, and $\mathbf{Fc_4}$ recorded in (10^{-5}−10^{-6} M) CH_2Cl_2.

absorption at 318 nm and a weaker absorption at 280 nm, which is similar to $\mathbf{A_2}$ but with higher intensity observed. $\mathbf{A_3}$ displays a highly overlapping absorption spectrum with that of $\mathbf{A_2B}$. The dependence of the electronic structure on the *syn*/*anti* relationship of the ferrocenyl fragments appears insignificant, which is in agreement with the reported results for the ferrocene-dehydroannulenes.[36] To further investigate the ring-size effect, the absorption spectrum of mixture $\mathbf{Fc_4}$ was obtained and showed a similar absorption pattern. Additionally, the much weaker absorption bands (around 450 nm) observed in these ferrocenyl compounds were attributed to ferrocene d-d transition.[71,72] Likely because ferrocene is commonly known as a luminescence quencher, no detectable fluorescence was observed from these four compounds in a CH_2Cl_2 solution.

In addition, we note that $\mathbf{A_2B}$ may have nonlinear optically relevant properties,[73,74] with the noncentrosymmetric space group ($P2_12_12_1$) that is required for second harmonic generation. As the excitation power remains constant, nonlinear optical (NLO) spectra of $\mathbf{A_2B}$ show clear second-harmonic generation (SHG) responses in a broad scope of pump wavelengths swept from 860 to 1040 nm (Figure 6a), with the incidence and detection angles set at 45° with respect to the surface normal. The largest SHG signal can be pumped at approximately 1040 nm for $\mathbf{A_2B}$. The quadratic correlation

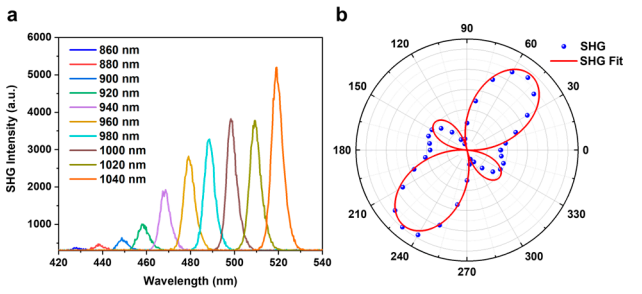

Figure 6. (a) NLO spectra of $\mathbf{A_2B}$ single crystals pumped at different wavelengths from 860 to 1040 nm. (b) Polarization dependence plot of the SHG signal of the $\mathbf{A_2B}$ single crystal with an incident wavelength of 1040 nm.

plot of the SHG intensity versus the incident laser power for the $\mathbf{A_2B}$ crystal at an 880 nm incident wavelength has a linear fitting slope of 1.99 (Figure S17). Next, the polarization dependence of the NLO signal is investigated (Figure 6b). The maximum value of the SHG response of the crystal occurs when the excitation beam is polarized in directions of 50° and 230°.

FRONTIER MOLECULAR ORBITALS

To further understand the effect of the orientation of ferrocenyl units in macrocycles, density functional theory (DFT) calculations were carried out. Geometry optimizations for the structures of $\mathbf{A_3}$ and $\mathbf{A_2B}$ were performed at the PBE0-D3(BJ)/Def2-SVP level of theory (Figure S18). It was found that $\mathbf{A_2B}$ is thermodynamically more stable than $\mathbf{A_3}$, with a difference of about 2.3 kcal mol^{-1}. Furthermore, time-dependent (TD)-DFT calculations were performed at the PBE0-D3(BJ)/Def2-SVP level of theory. $\mathbf{A_2B}$ and $\mathbf{A_3}$ exhibit similar orbital distributions (Figures S25 and 26), with the highest occupied molecular orbital (HOMO) delocalized along the entire backbone and the lowest unoccupied molecular orbital (LUMO) predominantly delocalized on the biphenyl moieties, indicating the formation of a π-conjugate system. Both compounds have HOMO levels of −5.63 eV, while the LUMO levels are −1.22 and −1.26 eV for $\mathbf{A_2B}$ and $\mathbf{A_3}$, respectively (Table S2). The simulated UV−vis absorption spectra of $\mathbf{A_2B}$ and $\mathbf{A_3}$, obtained through TD-DFT, are consistent with the experimental results. In both cases, the HOMO to LUMO transition is forbidden. In addition, the major absorption peaks (318 nm) originate from HOMO−1 to LUMO and HOMO to LUMO+1 transitions (f = 1.06), as well as from HOMO−2 to LUMO and HOMO to LUMO+2 (f = 0.90) (Figure 7), while the higher energy absorption peak (280 nm) is more complicated (see Tables S3 and S4).

The strain energies of $\mathbf{A_2B}$ and $\mathbf{A_3}$ were evaluated using homodesmotic reactions,[75] revealing that $\mathbf{A_2B}$ is slightly less strained (43 kcal mol^{-1}) than $\mathbf{A_3}$ (45 kcal mol^{-1}) (Scheme S1). This finding suggests that the main product being $\mathbf{A_2B}$ is likely due to its lower strain. These values are also much lower than that [9]CPP (66 kcal mol^{-1}).[75] To further analyze the strain distribution (Figure 8a), we employed the StrainViz program developed by Jasti et al.[76] The results indicate that $\mathbf{A_3}$ has more strain than $\mathbf{A_2B}$ in various aspects (Table S6).

In addition, the barriers of flipping three types of ferrocenyl units in $\mathbf{A_2B}$ and $\mathbf{A_3}$ were investigated. In all cases, two transition states (Ts) and one metastable state were identified. For example, in $\mathbf{A_3}$ (Figure 8b), the energy difference required to transition from the most stable structure to Ms1 is

https://doi.org/10.1021/prechem.3c00121
Precis. Chem. 2024, 2, 143−150

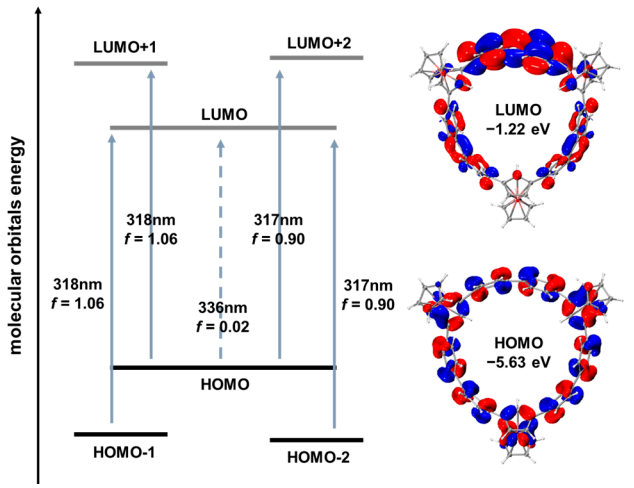

Figure 7. Qualitative energy diagram and frontier molecular orbitals of A_2B, calculated at the PBE0-D3(BJ)/Def2-SVP level of theory.

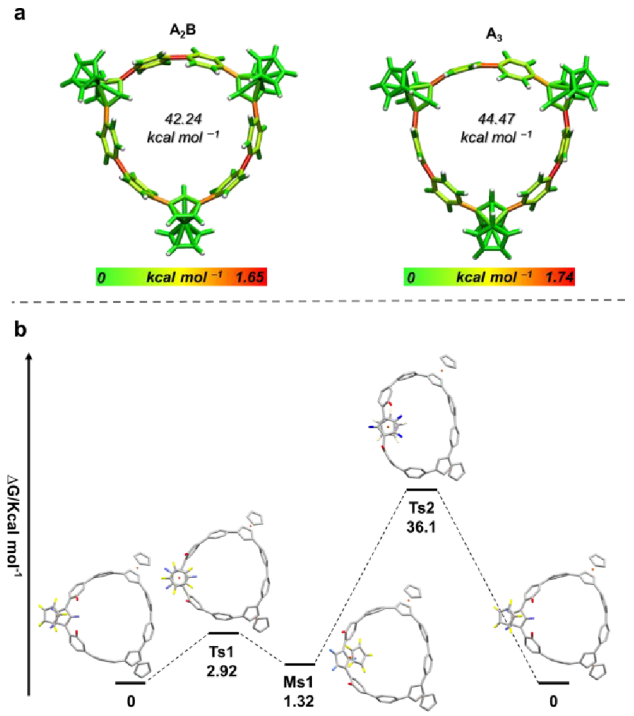

Figure 8. (a) Molecular strain energy for A_2B and A_3 calculated and visualized using StrainViz and (b) relative Gibbs free energy diagram of the ferrocenyl rotational barriers in A_3 (B3LYP/SDD, 6-31g(d); Transition State: Ts; Metastable State: Ms.).

approximately 2.92 kcal mol^{-1}. The Ts2, with an energy barrier of 36.1 kcal mol^{-1}, is associated with a change in the orientation of the ferrocenyl unit. This energy barrier suggests that the ferrocenyl unit is unlikely to cross at room temperature (see Figure S20−21 for detailed information on the energy barrier for A_2B).

In terms of future application, some insight into side-chain type ferrocene rings' coordination organometallic chemistry has been provided. The dissociation of ferrocene in main-chain ferrocene macrocycles leads to ring-opened linear products.[39−41] However, side-chain ferrocene macrocycles can form macrocycles embedded in Cp, which are more attractive for subsequent modification due to the metal coordination chemistry of the Cp unit. For example, Garbicz et al. recently reported that the Cp unit in side-chain macrocycle acts as a synthon for the construction of meso-tetraaryl-21-carbaporphyrin.[38] Notably, we observed signals of macrocyclic species shedding CpFe by MALDI FT-ICR MS (Figures S34−S36), which demonstrated that the side-chain ferrocene rings could be promising macrocyclic ligands for exploring organometallic chemistry in a well-defined curved radially conjugated macrocyclic environment.

CONCLUSIONS

In summary, new side-chain type ferrocene-based π-conjugated macrocycles have been successfully synthesized and analyzed in detail. The stereo configuration of the two cyclotrimers was unambiguously confirmed through single crystal X-ray diffraction. Notably, both macrocycles exhibit unique herringbone packing induced by ferrocene-to-ring host−guest interactions, suggesting potential applications in host−guest chemistry. UV−vis absorption spectroscopy and theoretical calculation indicate that the orientation of ferrocenyl units (*syn*/*anti*) has no significant effect on the electronic structure of these cyclic conjugated systems. Electrochemical measurements support these findings and also reveal a weak interaction between the redox centers. A_2B single crystals demonstrated second-order nonlinear optical properties. In addition, these rings have the potential to generate Cp-containing macrocycles, formed after Cp-FeCp breaking. Further studies are underway to exploit the coordination ability of the Cp-containing macrocycle as a curved π-conjugated macrocyclic ligands. Considering the recent advances in single-molecule electronics with conjugated cyclic structures,[77−79] the study of electronic transport performance of these new type macrocycles is ongoing as well.

ASSOCIATED CONTENT

Supporting Information

The Supporting Information is available free of charge at https://pubs.acs.org/doi/10.1021/prechem.3c00121.

Experimental procedures and characterization data for all compounds; electrochemistry, NLO measurements, UV−vis-NIR, VT-NMR experimental details, and computational results (PDF)

Crystallographic data for **2** (CIF)

Crystallographic data for A_2B (CIF)

Crystallographic data for A_3 (CIF)

AUTHOR INFORMATION

Corresponding Authors

Yuanming Li − *Key Laboratory of Molecule Synthesis and Function Discovery (Fujian Province University), College of Chemistry and Key Laboratory of Advanced Carbon-Based Functional Materials (Fujian Province University), College of Chemistry, Fuzhou University, Fuzhou 350108, China;* orcid.org/0000-0003-3180-1305; Email: yuanming.li@fzu.edu.cn

Yaofeng Yuan − *Key Laboratory of Molecule Synthesis and Function Discovery (Fujian Province University), College of Chemistry, Fuzhou University, Fuzhou 350108, China;* Email: yaofeng_yuan@fzu.edu.cn

Kenichiro Itami − *Institute of Transformative Bio-Molecules (WPI-ITbM), Nagoya University, Nagoya 464-8602, Japan;*

https://doi.org/10.1021/prechem.3c00121
Precis. Chem. 2024, 2, 143−150

orcid.org/0000-0001-5227-7894; Email: itami@chem.nagoya-u.ac.jp

Songhua Chen − *College of Chemistry and Material Science, Longyan University, Longyan 364012, China*; Email: songhua@iccas.ac.cn

Authors

Bin Lan − *Key Laboratory of Molecule Synthesis and Function Discovery (Fujian Province University), College of Chemistry, Fuzhou University, Fuzhou 350108, China*

Jindong Xu − *Key Laboratory of Molecule Synthesis and Function Discovery (Fujian Province University), College of Chemistry, Fuzhou University, Fuzhou 350108, China*

Lingyun Zhu − *Key Laboratory of Molecule Synthesis and Function Discovery (Fujian Province University), College of Chemistry, Fuzhou University, Fuzhou 350108, China*

Xinyu Chen − *Key Laboratory of Molecule Synthesis and Function Discovery (Fujian Province University), College of Chemistry, Fuzhou University, Fuzhou 350108, China*

Hideya Kono − *Institute of Transformative Bio-Molecules (WPI-ITbM), Nagoya University, Nagoya 464-8602, Japan*

Peihan Wang − *School of Materials Science and Engineering, National Institute for Advanced Materials, Nankai University, Tianjin 300350, China*

Xin Zuo − *Key Laboratory of Molecule Synthesis and Function Discovery (Fujian Province University), College of Chemistry, Fuzhou University, Fuzhou 350108, China*

Jianfeng Yan − *Key Laboratory of Molecule Synthesis and Function Discovery (Fujian Province University), College of Chemistry, Fuzhou University, Fuzhou 350108, China*

Akiko Yagi − *Institute of Transformative Bio-Molecules (WPI-ITbM), Nagoya University, Nagoya 464-8602, Japan*

Yongshen Zheng − *School of Materials Science and Engineering, National Institute for Advanced Materials, Nankai University, Tianjin 300350, China*

Complete contact information is available at: https://pubs.acs.org/10.1021/prechem.3c00121

Author Contributions

Bin Lan planned the experiments, synthesized and characterized the compounds with the help of Jindong Xu and Xin Zuo. Xinyu Chen, Hideya Kono, and Lingyun Zhu performed the DFT calculations. Peihan Wang, Yongshen Zheng, and Songhua Chen performed the nonlinear optical studies. Jianfeng Yan aided in interpreting the results and worked on the manuscript. Bin Lan wrote the original draft with input from all the coauthors. All authors discussed the results and contributed to the final manuscript. Yuanming Li, Kenichiro Itami, Yaofeng Yuan, and Akiko Yagi were involved in planning and supervised the project.

Notes

The authors declare no competing financial interest.

■ ACKNOWLEDGMENTS

This work was supported from National Natural Science Foundation of China (No. 22071025) and the Natural Science Fund of Fujian Province, China (No.2022J011152). We thank Prof. Xinxiong Li and Prof. Weiguo Huang for the single crystal measurement, Prof. Chaolumen, Prof. Jialiang Xu, Prof. Xiang Li, Prof. Ye Sha, and Xiangzhao Zhu for constructive criticism of the manuscript, and Professor Tan Yu for naming side-chain type ferrocene macrocycles.

■ REFERENCES

(1) Williams, K. A.; Boydston, A. J.; Bielawski, C. W. Main-chain organometallic polymers: synthetic strategies, applications, and perspectives. *Chem. Soc. Rev.* **2007**, *36*, 729−744.

(2) Hudson, R. D. A. Ferrocene polymers: current architectures, syntheses and utility. *J. Organomet. Chem.* **2001**, *637*−*639*, 47−69.

(3) Pietschnig, R. Polymers with pendant ferrocenes. *Chem. Soc. Rev.* **2016**, *45*, 5216−5231.

(4) Musgrave, R. A.; Russell, A. D.; Hayward, D. W.; Whittell, G. R.; Lawrence, P. G.; Gates, P. J.; Green, J. C.; Manners, I. Main-chain metallopolymers at the static−dynamic boundary based on nickelocene. *Nat. Chem.* **2017**, *9*, 743−750.

(5) Hudson, Z. M.; Lunn, D. J.; Winnik, M. A.; Manners, I. Colour-tunable fluorescent multiblock micelles. *Nat. Commun.* **2014**, *5*, 3372.

(6) Masson, G.; Herbert, D. E.; Whittell, G. R.; Holland, J. P.; Lough, A. J.; Green, J. C.; Manners, I. Synthesis and Reactivity of a Strained Silicon-Bridged [1]Ferrocenophanium Ion. *Angew. Chem., Int. Ed.* **2009**, *48*, 4961−4964.

(7) Lewis, S. E. Cycloparaphenylenes and related nanohoops. *Chem. Soc. Rev.* **2015**, *44*, 2221−2304.

(8) Darzi, E. R.; Jasti, R. The dynamic, size-dependent properties of [5]−[12]cycloparaphenylenes. *Chem. Soc. Rev.* **2015**, *44*, 6401−6410.

(9) Hermann, M.; Wassy, D.; Esser, B. Conjugated Nanohoops Incorporating Donor, Acceptor, Hetero- or Polycyclic Aromatics. *Angew. Chem., Int. Ed.* **2021**, *60*, 15743−15766.

(10) Li, Y.; Kono, H.; Maekawa, T.; Segawa, Y.; Yagi, A.; Itami, K. Chemical Synthesis of Carbon Nanorings and Nanobelts. *Acc. Mater. Res.* **2021**, *2*, 681−691.

(11) Wang, J.; Zhang, X.; Jia, H.; Wang, S.; Du, P. Large π-Extended and Curved Carbon Nanorings as Carbon Nanotube Segments. *Acc. Chem. Res.* **2021**, *54*, 4178−4190.

(12) Povie, G.; Segawa, Y.; Nishihara, T.; Miyauchi, Y.; Itami, K. Synthesis of a carbon nanobelt. *Science* **2017**, *356*, 172−175.

(13) Cheung, K. Y.; Gui, S.; Deng, C.; Liang, H.; Xia, Z.; Liu, Z.; Chi, L.; Miao, Q. Synthesis of Armchair and Chiral Carbon Nanobelts. *Chem.* **2019**, *5*, 838−847.

(14) Luan, Y.; Cong, H. Recent Synthetic Advances on π-Extended Carbon Nanohoops. *Synlett.* **2017**, *28*, 1383−1388.

(15) Esser, B.; Hermann, M. Buckling up zigzag nanobelts. *Nat. Chem.* **2021**, *13*, 209−211.

(16) Kaiser, K.; Scriven, L. M.; Schulz, F.; Gawel, P.; Gross, L.; Anderson, H. L. An sp-hybridized molecular carbon allotrope, cyclo[18]carbon. *Science* **2019**, *365*, 1299−1301.

(17) Scriven, L. M.; Kaiser, K.; Schulz, F.; Sterling, A. J.; Woltering, S. L.; Gawel, P.; Christensen, K. E.; Anderson, H. L.; Gross, L. Synthesis of Cyclo[18]carbon via Debromination of C18Br6. *J. Am. Chem. Soc.* **2020**, *142*, 12921−12924.

(18) Muraoka, T.; Kinbara, K.; Kobayashi, Y.; Aida, T. Light-Driven Open−Close Motion of Chiral Molecular Scissors. *J. Am. Chem. Soc.* **2003**, *125*, 5612−5613.

(19) Muraoka, T.; Kinbara, K.; Aida, T. Mechanical twisting of a guest by a photoresponsive host. *Nature* **2006**, *440*, 512−515.

(20) Aragonès, A. C.; Darwish, N.; Ciampi, S.; Jiang, L.; Roesch, R.; Ruiz, E.; Nijhuis, C. A.; Díez-Pérez, I. Control over Near-Ballistic Electron Transport through Formation of Parallel Pathways in a Single-Molecule Wire. *J. Am. Chem. Soc.* **2019**, *141*, 240−250.

(21) Moneo, A.; González-Orive, A.; Bock, S.; Fenero, M.; Herrer, I. L.; Milan, D. C.; Lorenzoni, M.; Nichols, R. J.; Cea, P.; Perez-Murano, F.; Low, P. J.; Martin, S. Towards molecular electronic devices based on 'all-carbon' wires. *Nanoscale.* **2018**, *10*, 14128−14138.

(22) Camarasa-Gómez, M.; Hernangómez-Pérez, D.; Inkpen, M. S.; Lovat, G.; Fung, E. D.; Roy, X.; Venkataraman, L.; Evers, F. Mechanically Tunable Quantum Interference in Ferrocene-Based Single-Molecule Junctions. *Nano Lett.* **2020**, *20*, 6381−6386.

(23) Xiao, C.; Wu, W.; Liang, W.; Zhou, D.; Kanagaraj, K.; Cheng, G.; Su, D.; Zhong, Z.; Chruma, J. J.; Yang, C. Redox-Triggered Chirality Switching and Guest-Capture/Release with a Pillar[6]arene-Based Molecular Universal Joint. *Angew. Chem., Int. Ed.* **2020**, *59*, 8094−8098.

(24) Xu, L.; Wang, Y.-X.; Chen, L.-J.; Yang, H.-B. Construction of multiferrocenyl metallacycles and metallacages via coordination-driven self-assembly: from structure to functions. *Chem. Soc. Rev.* **2015**, *44*, 2148−2167.
(25) Grossmann, B.; Heinze, J.; Herdtweck, E.; Köhler, F. H.; Nöth, H.; Schwenk, H.; Spiegler, M.; Wachter, W.; Weber, B. Seven Doubly Bridged Ferrocene Units in a Cycle. *Angew. Chem., Int. Ed.* **1997**, *36*, 387−389.
(26) Herbert, D. E.; Gilroy, J. B.; Chan, W. Y.; Chabanne, L.; Staubitz, A.; Lough, A. J.; Manners, I. Redox-Active Metallomacrocycles and Cyclic Metallopolymers: Photocontrolled Ring-Opening Oligomerization and Polymerization of Silicon-Bridged [1]-Ferrocenophanes Using Substitutionally-Labile Lewis Bases as Initiators. *J. Am. Chem. Soc.* **2009**, *131*, 14958−14968.
(27) Chan, W. Y.; Lough, A. J.; Manners, I. Organometallic Macrocycles and Cyclic Polymers by the Bipyridine-Initiated Photolytic Ring Opening of a Silicon-Bridged [1]Ferrocenophane. *Angew. Chem., Int. Ed.* **2007**, *46*, 9069−9072.
(28) Winter, T.; Haider, W.; Schießer, A.; Presser, V.; Gallei, M.; Schäfer, A. Rings and Chains: Synthesis and Characterization of Polyferrocenylmethylene. *Macromol. Rapid Commun.* **2021**, *42*, 2000738.
(29) Inkpen, M. S.; Scheerer, S.; Linseis, M.; White, A. J. P.; Winter, R. F.; Albrecht, T.; Long, N. J. Oligomeric ferrocene rings. *Nat. Chem.* **2016**, *8*, 825−830.
(30) Simkowa, I.; Latos-Grażyński, L.; Stępień, M. π Conjugation Transmitted across a d-Electron Metallocene in Ferrocenothiaporphyrin Macrocycles. *Angew. Chem., Int. Ed.* **2010**, *49*, 7665−7669.
(31) Metzelaars, M.; Schleicher, S.; Hattori, T.; Borca, B.; Matthes, F.; Sanz, S.; Bürgler, D. E.; Rawson, J.; Schneider, C. M.; Kögerler, P. Cyclophane with eclipsed pyrene units enables construction of spin interfaces with chemical accuracy. *Chem. Sci.* **2021**, *12*, 8430−8437.
(32) Metzelaars, M.; Sanz, S.; Rawson, J.; Hartmann, R.; Schneider, C. M.; Kögerler, P. Fusing pyrene and ferrocene into a chiral, redox-active triangle. *Chem. Commun.* **2021**, *57*, 6660−6663.
(33) Wilson, L. E.; Hassenrück, C.; Winter, R. F.; White, A. J. P.; Albrecht, T.; Long, N. J. Ferrocene- and Biferrocene-Containing Macrocycles towards Single-Molecule Electronics. *Angew. Chem., Int. Ed.* **2017**, *56*, 6838−6842.
(34) Hoffmann, V.; le Pleux, L.; Häussinger, D.; Unke, O. T.; Prescimone, A.; Mayor, M. Deltoid versus Rhomboid: Controlling the Shape of Bis-ferrocene Macrocycles by the Bulkiness of the Substituents. *Organometallics.* **2017**, *36*, 858−866.
(35) Sheppard, S. A.; Bennett, T. L. R.; Long, N. J. Development and Characterisation of Highly Conjugated Functionalised Ferrocenylene Macrocycles. *Eur. J. Inorg. Chem.* **2022**, *2022*, e202200055.
(36) Bunz, U. H. F.; Roidl, G.; Altmann, M.; Enkelmann, V.; Shimizu, K. D. Synthesis and Structural Characterization of Novel Organometallic Dehydroannulenes with Fused CpCo-Cyclobutadiene and Ferrocene Units Including a Cyclic Fullerenyne Segment. *J. Am. Chem. Soc.* **1999**, *121*, 10719−10726.
(37) Hisatome, M.; Tachikawa, O.; Sashō, M.; Yamakawa, K. Organometallic compounds: XXXII. Syntheses of 1,3-disubstituted ferrocenes and intermolecular (1,3)ferrocenophanes. *J. Organomet. Chem.* **1981**, *217*, C17−C20.
(38) Garbicz, M.; Latos-Grażyński, L. A meso-Tetraaryl-21-carbaporphyrin: Incorporation of a Cyclopentadiene Unit into a Porphyrin Architecture. *Angew. Chem., Int. Ed.* **2019**, *58*, 6089−6093.
(39) Di Giannantonio, M.; Ayer, M. A.; Verde-Sesto, E.; Lattuada, M.; Weder, C.; Fromm, K. M. Triggered Metal Ion Release and Oxidation: Ferrocene as a Mechanophore in Polymers. *Angew. Chem., Int. Ed.* **2018**, *57*, 11445−11450.
(40) Sha, Y.; Zhang, Y.; Xu, E.; Wang, Z.; Zhu, T.; Craig, S. L.; Tang, C. Quantitative and Mechanistic Mechanochemistry in Ferrocene Dissociation. *ACS Macro Lett.* **2018**, *7*, 1174−1179.
(41) Zhang, Y.; Wang, Z.; Kouznetsova, T. B.; Sha, Y.; Xu, E.; Shannahan, L.; Fermen-Coker, M.; Lin, Y.; Tang, C.; Craig, S. L. Distal conformational locks on ferrocene mechanophores guide reaction pathways for increased mechanochemical reactivity. *Nat. Chem.* **2021**, *13*, 56−62.
(42) Katz, T. J.; Pesti, J. The synthesis of a helical ferrocene. *J. Am. Chem. Soc.* **1982**, *104*, 346−347.
(43) Amaya, T.; Takahashi, Y.; Moriuchi, T.; Hirao, T. Sumanenyl Metallocenes: Synthesis and Structure of Mono- and Trinuclear Zirconocene Complexes. *J. Am. Chem. Soc.* **2014**, *136*, 12794−12798.
(44) Jiang, H.-W.; Tanaka, T.; Mori, H.; Park, K. H.; Kim, D.; Osuka, A. Cyclic 2,12-Porphyrinylene Nanorings as a Porphyrin Analogue of Cycloparaphenylenes. *J. Am. Chem. Soc.* **2015**, *137*, 2219−2222.
(45) Jiang, H.-W.; Tanaka, T.; Kim, T.; Sung, Y. M.; Mori, H.; Kim, D.; Osuka, A. Synthesis of [n]Cyclo-5,15-porphyrinylene-4,4′-biphenylenes Displaying Size-Dependent Excitation-Energy Hopping. *Angew. Chem., Int. Ed.* **2015**, *54*, 15197−15201.
(46) Xu, Y.; Gsänger, S.; Minameyer, M. B.; Imaz, I.; Maspoch, D.; Shyshov, O.; Schwer, F.; Ribas, X.; Drewello, T.; Meyer, B.; von Delius, M. Highly Strained, Radially π-Conjugated Porphyrinylene Nanohoops. *J. Am. Chem. Soc.* **2019**, *141*, 18500−18507.
(47) Stawski, W.; Van Raden, J. M.; Patrick, C. W.; Horton, P. N.; Coles, S. J.; Anderson, H. L. Strained Porphyrin Tape−Cycloparaphenylene Hybrid Nanorings. *Org. Lett.* **2023**, *25*, 378−383.
(48) Kubota, N.; Segawa, Y.; Itami, K. η^6-Cycloparaphenylene Transition Metal Complexes: Synthesis, Structure, Photophysical Properties, and Application to the Selective Monofunctionalization of Cycloparaphenylenes. *J. Am. Chem. Soc.* **2015**, *137*, 1356−1361.
(49) Kayahara, E.; Patel, V. K.; Mercier, A.; Kündig, E. P.; Yamago, S. Regioselective Synthesis and Characterization of Multinuclear Convex-Bound Ruthenium-[n]Cycloparaphenylene (n = 5 and 6) Complexes. *Angew. Chem., Int. Ed.* **2016**, *55*, 302−306.
(50) Van Raden, J. M.; Louie, S.; Zakharov, L. N.; Jasti, R. 2,2′-Bipyridyl-Embedded Cycloparaphenylenes as a General Strategy To Investigate Nanohoop-Based Coordination Complexes. *J. Am. Chem. Soc.* **2017**, *139*, 2936−2939.
(51) Majewski, M. A.; Stawski, W.; Van Raden, J. M.; Clarke, M.; Hart, J.; O'Shea, J. N.; Saywell, A.; Anderson, H. L. Covalent Template-Directed Synthesis of a Spoked 18-Porphyrin Nanoring**. *Angew. Chem., Int. Ed.* **2023**, *62*, e202302114.
(52) Heras Ojea, M. J.; Van Raden, J. M.; Louie, S.; Collins, R.; Pividori, D.; Cirera, J.; Meyer, K.; Jasti, R.; Layfield, R. A. Spin-Crossover Properties of an Iron(II) Coordination Nanohoop. *Angew. Chem., Int. Ed.* **2021**, *60*, 3515−3518.
(53) Fuhrmann, G.; Debaerdemaeker, T.; Bäuerle, P. C−C bond formation through oxidatively induced elimination of platinum complexes—A novel approach towards conjugated macrocycles. *Chem. Commun.* **2003**, 948−949.
(54) Zhang, F.; Götz, G.; Winkler, H. D. F.; Schalley, C. A.; Bäuerle, P. Giant Cyclo[n]thiophenes with Extended π Conjugation. *Angew. Chem., Int. Ed.* **2009**, *48*, 6632−6635.
(55) Yamago, S.; Watanabe, Y.; Iwamoto, T. Synthesis of [8]Cycloparaphenylene from a Square-Shaped Tetranuclear Platinum Complex. *Angew. Chem., Int. Ed.* **2010**, *49*, 757−759.
(56) Hitosugi, S.; Nakanishi, W.; Yamasaki, T.; Isobe, H. Bottom-up synthesis of finite models of helical (n,m)-single-wall carbon nanotubes. *Nat. Commun.* **2011**, *2*, 492.
(57) Zhao, H.; Ma, Y.-C.; Cao, L.; Huang, S.; Zhang, J.-P.; Yan, X. Synthesis and Photophysical Properties of Chalcophenes-Embedded Cycloparaphenylenes. *J. Org. Chem.* **2019**, *84*, 5230−5235.
(58) Zirakzadeh, A.; Herlein, A.; Groß, M. A.; Mereiter, K.; Wang, Y.; Weissensteiner, W. Halide-Mediated Ortho-Deprotonation Reactions Applied to the Synthesis of 1,2- and 1,3-Disubstituted Ferrocene Derivatives. *Organometallics.* **2015**, *34*, 3820−3832.
(59) Brandl, M.; Weiss, M. S.; Jabs, A.; Sühnel, J.; Hilgenfeld, R. C-h···π-interactions in proteins. *J. Mol. Biol.* **2001**, *307*, 357−377.
(60) Nishio, M.; Umezawa, Y.; Hirota, M.; Takeuchi, Y. The CH/π interaction: Significance in molecular recognition. *Tetrahedron.* **1995**, *51*, 8665−8701.

(61) Kwon, H.; Newell, B. S.; Bruns, C. J. Redox-switchable host–guest complexes of metallocenes and [8]cycloparaphenylene. *Nanoscale* **2022**, *14*, 14276–14285.
(62) Liu, C. Y.; Meng, M. Introduction and Fundamentals of Mixed-Valence Chemistry. *Mixed-Valence Systems* **2023**, 1–43.
(63) Santi, S.; Orian, L.; Donoli, A.; Bisello, A.; Scapinello, M.; Benetollo, F.; Ganis, P.; Ceccon, A. Synthesis of the Prototypical Cyclic Metallocene Triad: Mixed-Valence Properties of [(FeCp)3-(trindenyl)] Isomers. *Angew. Chem., Int. Ed.* **2008**, *47*, 5331–5334.
(64) Hildebrandt, A.; Miesel, D.; Lang, H. Electrostatic interactions within mixed-valent compounds. *Coord. Chem. Rev.* **2018**, *371*, 56–66.
(65) Geiger, W. E.; Barrière, F. Organometallic Electrochemistry Based on Electrolytes Containing Weakly-Coordinating Fluoroarylborate Anions. *Acc. Chem. Res.* **2010**, *43*, 1030–1039.
(66) Barrière, F.; Geiger, W. E. Use of Weakly Coordinating Anions to Develop an Integrated Approach to the Tuning of $\Delta E_{1/2}$ Values by Medium Effects. *J. Am. Chem. Soc.* **2006**, *128*, 3980–3989.
(67) LeSuer, R. J.; Buttolph, C.; Geiger, W. E. Comparison of the Conductivity Properties of the Tetrabutylammonium Salt of Tetrakis-(pentafluorophenyl)borate Anion with Those of Traditional Supporting Electrolyte Anions in Nonaqueous Solvents. *Anal. Chem.* **2004**, *76*, 6395–6401.
(68) D'Alessandro, D. M.; Keene, F. R. Current trends and future challenges in the experimental, theoretical and computational analysis of intervalence charge transfer (IVCT) transitions. *Chem. Soc. Rev.* **2006**, *35*, 424–440.
(69) Hildebrandt, A.; Lang, H. (Multi)ferrocenyl Five-Membered Heterocycles: Excellent Connecting Units for Electron Transfer Studies. *Organometallics* **2013**, *32*, 5640–5653.
(70) Santi, S.; Orian, L.; Durante, C.; Bencze, E. Z.; Bisello, A.; Donoli, A.; Ceccon, A.; Benetollo, F.; Crociani, L. Metal–Metal Electronic Coupling in syn and anti Stereoisomers of Mixed-Valent $(FeCp)_2$-, $(RhL_2)_2$-, and $(FeCp)(RhL_2)$-as-Indacenediide Ions. *Chem.—Eur. J.* **2007**, *13*, 7933–7947.
(71) Gray, H. B.; Sohn, Y. S.; Hendrickson, N. Electronic structure of metallocenes. *J. Am. Chem. Soc.* **1971**, *93*, 3603–3612.
(72) Cuffe, L.; Hudson, R. D. A.; Gallagher, J. F.; Jennings, S.; McAdam, C. J.; Connelly, R. B. T.; Manning, A. R.; Robinson, B. H.; Simpson, J. Synthesis, Structure, and Redox Chemistry of Ethenyl and Ethynyl Ferrocene Polyaromatic Dyads. *Organometallics.* **2005**, *24*, 2051–2060.
(73) Kaur, S.; Kaur, M.; Kaur, P.; Clays, K.; Singh, K. Ferrocene chromophores continue to inspire. Fine-tuning and switching of the second-order nonlinear optical response. *Coord. Chem. Rev.* **2017**, *343*, 185–219.
(74) Shi, R.; Han, X.; Cheng, P.; Xin, M.; Xu, J. Self-Assembled Nonlinear Optical Crystals Based on an Asymmetric Fluorenone Derivative. *Cryst. Growth Des.* **2022**, *22*, 3998–4004.
(75) Segawa, Y.; Omachi, H.; Itami, K. Theoretical Studies on the Structures and Strain Energies of Cycloparaphenylenes. *Org. Lett.* **2010**, *12*, 2262–2265.
(76) Colwell, C. E.; Price, T. W.; Stauch, T.; Jasti, R. Strain visualization for strained macrocycles. *Chem. Sci.* **2020**, *11*, 3923–3930.
(77) Lin, J.; Lv, Y.; Song, K.; Song, X.; Zang, H.; Du, P.; Zang, Y.; Zhu, D. Cleavage of non-polar $C(sp^2)$–$C(sp^2)$ bonds in cycloparaphenylenes via electric field-catalyzed electrophilic aromatic substitution. *Nat. Commun.* **2023**, *14*, 293.
(78) Lv, Y.; Lin, J.; Song, K.; Song, X.; Zang, H.; Zang, Y.; Zhu, D. Single cycloparaphenylene molecule devices: Achieving large conductance modulation via tuning radial π-conjugation. *Sci. Adv.* **2021**, *7*, eabk3095.
(79) Lin, J.; Wang, S.; Zhang, F.; Yang, B.; Du, P.; Chen, C.; Zang, Y.; Zhu, D. Highly efficient charge transport across carbon nanobelts. *Sci. Adv.* **2022**, *8*, eade4692.

https://doi.org/10.1021/prechem.3c00121
Precis. Chem. 2024, 2, 143–150